In Vitro Evolution of a Peptide with a Hematite Binding Motif That May Constitute a Natural Metal-Oxide Binding Archetype

BRIAN H. LOWER,*,†,‡
ROBERTO D. LINS,†
ZACHERY OESTREICHER,§
TJERK P. STRAATSMA,†
MICHAEL F. HOCHELLA JR.,||
LIANG SHI,† AND STEVEN K. LOWER§

Pacific Northwest National Laboratory, Richland, Washington 99352, The Ohio State University, 275 Mendenhall Laboratory, Columbus, Ohio 43210, and Virginia Tech, Blacksburg, Virginia 24061

Received October 24, 2007. Revised manuscript received February 29, 2008. Accepted March 4, 2008.

Phage-display technology was used to evolve peptides that selectively bind to the metal-oxide hematite (Fe_2O_3) from a library of approximately 3 billion different polypeptides. The sequences of these peptides contained the highly conserved amino acid motif, Ser/Thr-hydrophobic/aromatic-Ser/Thr-Pro-Ser/Thr. To better understand the nature of the peptide−metal oxide binding demonstrated by these experiments, molecular dynamics simulations were carried out for Ser-Pro-Ser at a hematite surface. These simulations show that hydrogen bonding occurs between the two serine amino acids and the hydroxylated hematite surface and that the presence of proline between the hydroxide residues restricts the peptide flexibility, thereby inducing a structural-binding motif. A search of published sequence data revealed that the binding motif (Ser/Thr-Pro-Ser/Thr) is adjacent to the terminal heme-binding domain of both OmcA and MtrC, which are outer membrane cytochromes from the metal-reducing bacterium *Shewanella oneidensis* MR-1. The entire five amino acid consensus sequence (Ser/Thr-hydrophobic/aromatic-Ser/Thr-Pro-Ser/Thr) was also found as multiple copies in the primary sequences of metal-oxide binding proteins Sil1 and Sil2 from *Thalassiosira pseudonana*. We suggest that this motif constitutes a natural metal-oxide binding archetype that could be exploited in enzyme-based biofuel cell design and approaches to synthesize tailored metal-oxide nanostructures.

Introduction

Billions of years ago, primitive prokaryotic cells evolved the protein machinery to use solid inorganic phases (e.g., iron oxides) as terminal electron acceptors (*1, 2*). Now, humans are exploiting this feat by using metal-reducing bacteria to form microbial fuel cells, a potential source of green energy (*3, 4*). In a microbial fuel cell, the microorganism converts dissolved organic matter (electron donor) into electricity by using an electrode as a terminal electron acceptor (*5*). Recent work has shown that biofuel cells can even be created by coating an iron-oxide electrode (i.e., hematite) with proteins purified from metal-reducing bacteria (*6, 7*). In this type of biofuel cell, redox-active enzymes are immobilized onto metal-oxide electrodes, and soluble cofactors (e.g., NADH) are used to reduce the enzymes. The reduced enzymes then catalyze the reduction of the metal-oxide electrode, thereby generating an electrical current.

The enzyme-based fuel cells are an intriguing form of green energy because of the small size of proteins, the diversity of microbial enzymes, the high turnover rates associated with such enzymes, and the variety of potential metal oxide electrodes. However, more experiments are necessary before the enzyme-based fuel cells reach the accepted status of the microbial fuel cell. A critical step in the development of enzyme-based fuel cells is the attachment of a redox-active enzyme onto an electrode surface in a manner that promotes efficient electron transfer (*8, 9*). One possible approach is the development of electrode-specific tags that are engineered into the primary amino acid sequence of the redox-active enzyme. Such tags could be adapted or designed to bind to a specific electrode surface using recombinant DNA technology.

Here, we directed the evolution of electrode-specific peptides using phage-display technology (*10*) to screen billions of random peptide sequences for those peptides displaying a selective affinity for the metal oxide hematite (α-Fe_2O_3). From the conserved amino acid sequences of these hematite-binding peptides we were able to determine a hematite-binding motif. Molecular dynamics simulations were then used to examine the molecular-scale mechanism of binding that occurred between this amino acid motif and a hematite surface. In addition, we discovered that this conserved hematite-binding motif is contained within the primary sequence of two decaheme cytochromes (OmcA and MtrC) from the metal reducing bacterium *Shewanella oneidensis* MR-1 (*11*). We also discovered that the conserved hematite-binding motif displays sequence features that are identical to metal-oxide binding proteins/peptides called silaffins, which have been shown to control SiO_2 deposition in vitro and to act as macromolecular templates for mediating biosilica nanopatterning in diatoms (*12*−*15*).

Experimental Section

Natural hematite (from Casa de Pedra, Congonhas do Campo, Minas Gerais, Brazil) was crushed in a mill, passed through a 45 μm sieve, cleaned of advantageous carbon (*16*), and analyzed by X-ray diffraction to confirm its identity. The hematite particles were then reacted with a Ph.D.-12 Phage Display Peptide Library (New England BioLabs; technical reference available at www.neb.com), which contained approximately 3×10^9 random peptides. Each peptide was 12 amino acids in length and fused to the N-terminus of the pIII coat protein of M13 bacteriophage (*17*). The M13 bacteriophage itself consisted of a single-stranded DNA core surrounded by a proteinaceous coat of five different types of coat proteins (including pIII). Each phage particle expressed ("displayed") 5 copies of the pIII coat protein/fused random peptide, which extends outward from the virus particle 10−16 nm. This arrangement thereby established a direct linkage between the peptide-mineral interaction (i.e., phenotype) and DNA encoding this interaction (i.e., genotype).

* Corresponding author e-mail: lower.30@osu.edu; phone: (614) 292-8522; fax: (614) 292-7432.
† Pacific Northwest National Laboratory.
‡ Current Address: The Ohio State University, 210 Kottman Hall, Columbus, Ohio 43210.
§ The Ohio State University.
|| Virginia Tech.

10.1021/es702688c CCC: $40.75
Published on Web 04/18/2008

The phage library was exposed to approximately 2.0 mg of hematite in Tris-buffered saline (TBS; pH 7.5) within 2.0 mL microcentrifuge tubes. The buffer contained 0.1% (v/v) Tween-20 to prevent nonspecific interactions. After mixing at room temperature, nonbinding phage were removed from the mineral by washing 10 times in TBS, pH 7.5, containing 0.1−0.5% (v/v) Tween-20. Bound phage were eluted from the mineral with the addition of 0.2 M Glycine-HCl (pH 2.2), transferred to a fresh tube, and neutralized with 1 M Tris-HCl (pH 9.1). The mineral-binding phage were titered, phage were amplified, and this entire process was repeated two more times using fresh mineral sample each time.

Following each round of hematite exposure, twenty phage plaques containing a random peptide insert were selected, and their DNA was sequenced. From these sequences, we determined the mineral-binding motif (i.e., amino acid sequence) that allowed the phage to bind hematite. A control experiment was also conducted using microcentrifuge tubes that lacked hematite.

Molecular simulations of peptide-mineral interactions were performed using the AMBER96 force field (*18*) in conjunction with the parallel version of the NWChem-4.7 program (*19*). An AMBER-compatible atomistic model of the fully hydroxylated oxygen-terminated hematite (001) surface was developed by empirical optimization of the point charges and van der Waals parameters following a similar procedure described in Lins and Hunenberger (*20*). The choice of the (001) surface was based on the fact that this surface is one of the most abundant hematite surfaces and has been the subject of numerous studies in aqueous solutions (*21, 22*). Furthermore, its unit cell characteristics allowed us to build a slab with α, β, and γ angles equal to 90° such that we could treat it, computationally, as an infinite mineral surface layer. The (001) surface was terminated with oxygen atoms because O-terminated domains have been experimentally observed and theoretically predicted (*21, 23−25*). In addition, Liu et al. (*26*) showed that low water vapor pressure ($\sim 10^{-4}$ Torr) was sufficient for full hydroxylation of the oxygen surface to occur; therefore, for our model, a fully hydroxylated oxygen-terminated hematite (001) surface was used.

The model was solvated and equilibrated for 5 ns. The water molecules were removed and the double (N- and C-terminal) acetylated peptide sequences Ser-Pro-Ser and Ser-Gly-Ser were placed ~10 Å away from the equilibrated hematite surface. A short (i.e., 500 ps) molecular dynamics simulation was performed to promote a quick approach of the peptides to the mineral surface. The latter had its atomic coordinates constrained to avoid artificial distortions due to the absence of the solvent. Once the peptides have reached the mineral surface, the systems were fully solvated, and energy was optimized using up to 500 steps of steepest descent. Production runs were simulated for 5 ns.

All molecular dynamics runs were carried out in the isothermal−isobaric ensemble with velocity reassignments every 0.4 ps. The temperature was maintained at 300 K by weak coupling between the solute and solvent (separately) to a heat bath (*27*) with a relaxation time of 0.1 ps. The pressure was kept at 1.025×10^5 Pascal using weak coupling to a pressure bath (*27*) via isotropic coordinate scaling with a relaxation time of 0.1 ps. Long-range electrostatic interactions were handled using the smooth particle mesh Ewald (SPME) method (*28*). A cutoff of 1.0 nm was used for the short-range nonbonded interactions (van der Waals and real-space electrostatic contribution). The SHAKE (*29*) algorithm was applied to constrain all bonds involving a hydrogen atom, and a 2 fs time step was used to integrate the equations of motion based on the leapfrog algorithm (*30*). The atomic coordinates of the iron and oxygen atoms in the hematite surface were constrained to ensure the integrity of the mineral structure upon peptide interaction. Trajectory frames were recorded every 0.2 ps for analysis.

Peptide	Amino Acid Sequence												
1	–	Q	M	D	T	S	T	S	L	A	P	S	R	–
2	–	V	P	F	T	L	Q	T	R	S	L	S	D	–
3	T	V	T	P	S	N	I	S	F	T	P	S	–	–
4	–	A	S	T	L	I	N	P	L	S	I	S	L	–
5	–	–	A	G	S	T	A	S	V	T	P	A	K	H
6	Q	M	A	N	S	V	M	P	L	S	W	T	–	–
7	–	Y	A	H	S	H	D	K	Y	H	P	N	–	–
8	–	N	Q	S	P	H	S	T	Y	T	L	K	P	–
9	–	–	H	N	Y	P	Q	S	Y	R	P	P	I	V
10	–	T	D	N	N	T	T	A	L	T	P	S	H	–
11	T	M	N	N	T	T	A	T	V	S	P	S	–	–
12	F	Q	K	Q	T	N	Q	S	V	S	V	S	–	–
13	–	V	H	M	T	P	T	N	L	T	P	N	L	–
14	–	T	F	S	Y	H	N	S	N	S	P	T	–	–
15	–	V	P	D	H	Q	V	S	Y	T	L	S	R	–
16	–	I	F	H	S	H	A	S	L	S	P	N	S	–
17	A	D	N	A	N	V	S	T	L	H	P	T	–	–
18	V	N	Q	Q	P	S	S	A	F	S	P	S	–	–
19	–	–	L	S	T	V	Q	T	I	S	P	S	N	H
20	D	M	N	H	T	K	S	S	Y	N	P	S	–	–
Motif	–	–	–	$	S/T	$	$	S/T	#	S/T	P	S/T	–	–
%	–	–	–	65	60	60	65	70	90	75	70	70	–	–

FIGURE 1. Amino acid sequences from each of the twenty sequenced phage clones that are bound to hematite (Fe_2O_3) following the third round of selection. Positions having conserved amino acid residues are underlined. Nonpolar, hydrophobic, and aromatic amino acids (A, F, I, L, M, V, W, Y) are shown in red. Polar charged amino acids (D, E, K, R) are shown in blue. Polar uncharged amino acids (C, H, N, Q, S, T) are shown in green. Glycine (G) is shown in black, and proline (P) is shown in purple. The determined hematite-binding motif is given below the amino acid sequences. Other symbols used: $, postions conserving polar uncharged residues; #, positions conserving nonpolar hydrophobic (including aromatic) residues; %, percent of occurrence that a conserved amino acid residue was observed at a specific location in the peptides.

Results and Discussion

Phage were reacted with hematite over the course of three sequential binding experiments (see Experimental Section). The stringency of each binding experiment was increased by increasing the concentration of Tween-20 (used to prevent nonspecific binding) from 0.1 to 0.5% in rounds two and three. After each round of phage selection, 20 hematite-binding phage were isolated at random. The DNA within the phage was sequenced to determine the sequence of the 12-amino acid peptide expressed on the surface of the phage. These peptide sequences were manually aligned to identify amino acid residues that were conserved among the peptides. An amino acid was considered to be conserved (i.e., essential for hematite binding) if it, or another amino acid residue having similar physicochemical properties (*31*), was observed at a specific location in a peptide sequence in at least 12 of the 20 peptides (60%) analyzed. After the third round of phage selection, the peptides displayed a clear consensus sequence defined by a motif of nine amino acids (Figure 1). This motif consisted of serine/threonine residues separated by polar or hydrophobic/aromatic residues or, in the case of the serine/

TABLE 1. Expected and Observed Distribution of Amino Acids Contained within the 12-Amino Acid Peptides That Were Bound to Hematite[a]

	polar uncharged C, H, N, Q, S, T	polar charged D, E, K, R	nonpolar hydrophobic aromatic A, F, I, L, M, V, W, Y	proline P	serine and threonine S, T
Ph.D.-12 library (expected)[b]	3.7(31%)	2.3(19%)	4.5(38%)	0.7(6%)	1.9(16%)
hematite (observed)	6.4 ± 1.2(53%)	0.8 ± 0.7(7%)	3.4 ± 1.1(28%)	1.3 ± 0.6(11%)	3.9 ± 1.3(32%)

[a] Shown are the expected distributions of amino acids for the peptides of the random Ph.D.-12 library and the observed distribution of amino acids for those peptides that bound to hematite. The first number in each row corresponds to the average number of amino acids per 12-amino acid peptide ± standard deviation; the number in parentheses corresponds to the average frequency of amino acids. [b] The expected frequency data were obtained from New England BioLabs and equals the number of codons for an amino acid ÷ 32 codons × 100%. Glycine (G) had an expected frequency of 6% for the random Ph.D.-12 library but was not included in this table since it was not found in significant quantities (i.e., Gly was observed once in one peptide; see Figure 1) in the hematite-binding peptides.

threonine residues located at the C-terminus, separated by a highly conserved proline (Figure 1). The control experiment (phage placed in microcentrifuge tubes lacking hematite) did not yield the conserved motif shown in Figure 1. In fact, the control phage did not exhibit any type of consensus sequence.

We chose to stop after the third round of phage-selection for the following reasons. First, since the library contains ~2×10^9 different clones, the eluted pool of phage should, in theory, be fully enriched in favor of binding sequences after only 2 or 3 rounds (New England BioLabs). Once this point is reached, further rounds of amplification and panning will result only in selection of phage that have a growth advantage over the Ph.D.-12 library phage (New England BioLabs). For example, vanishingly small levels of contaminating environmental wild-type phage (less than one part per billion) will completely overtake the pool if too many rounds of amplification are carried out, regardless of the strength of the in vitro selection (New England BioLabs). Second, the stringency of the binding experiments was increased by increasing the concentration of Tween-20 (used to prevent nonspecific interactions) from 0.1% in the first round of binding to 0.5% in the second and third rounds. This resulted in an increased number of "conserved" amino acids among the phage. Specifically, phage from the first, second, and third rounds of selective binding experiments contained on average 2.2, 5.0, and 6.2 amino acids, respectively, of the motif shown in Figure 1. Therefore, the third round of phage selection was deemed acceptable as it resulted in a comparably smaller increase in the number of amino acids within the conserved motif. That is, the first round yielded 24% (2.2 out of 9) of the amino acids in the conserved motif (Figure 1), whereas rounds two and three both had a significantly greater number of conserved residues than round one, but both were similar at 56% and 69%, respectively. Finally, the control experiments (phage placed in microcentrifuge tubes lacking hematite) did not yield the conserved motif shown in Figure 1.

To verify that the conserved amino acid motif was required for hematite binding, we examined the binding efficiency of one of the phage peptides shown in Figure 1. Phage No. 19 (Figure 1) was chosen because it contained eight of the nine amino acids conserved within the hematite-binding motif, which was the most for any of the peptides shown in Figure 1. Phage No. 19 (Figure 1), which expressed LSTVQTISPSNH, was amplified as described in the Experimental Section. Approximately 10^9 of these phage particles were incubated with 2.0 mg of hematite in buffer containing TBS (pH 7.5) and 0.5% Tween-20. After mixing at room temperature for 15 min, nonbinding phage were removed from the mineral by washing 10 times in fresh buffer. Bound phage were eluted from the mineral with the addition of 0.2 M glycine-HCl (pH 2.2), transferred to a fresh tube, and neutralized with 1 M Tris-HCl (pH 9.1). Detection of the bound phage was possible because the cloning vector (M13mp19) of the Ph.D.-12 Library phage carries the *lacZ*α gene. Therefore, phage plaques appear blue when plated on media containing Xgal and IPTG. The hematite-eluted phage were titered on LB/IPTG/Xgal plates, and the number of blue plaques were counted and then multiplied by the dilution factor. By dividing this number by the total number of phage incubated with the hematite (i.e., 10^9), we determined the percent of phage that bound to the hematite. For these experiments, 96% of phage No. 19 particles bound to hematite.

The same experiment was conducted for a control phage that expressed the peptide GHANHQAWNNLA. This phage was selected as a control because, like phage No. 19, it lacked polar charged residues, but unlike phage No. 19, it did not contain the hematite-binding motif shown in Figure 1, nor did it contain Ser, Thr, or Pro residues. For this control experiment, less than 0.5% (our limit of detection) of the control phage bound to the hematite. This confirmed the results of our phage selection experiments. It revealed that the conserved hematite-binding motif contained within the 20 peptides shown in Figure 1 is required for binding between the phage and hematite.

Table 1 compares the amino acids contained within the peptide sequences bound to hematite versus the expected peptide sequences for the random phage library. Hematite-binding phage displayed peptide sequences composed of mostly polar uncharged amino acids (53%; see Table 1). For comparison, polar uncharged amino acids are expected to constitute only 31% of the functional groups in a random 12 amino acid peptide (Table 1). The observed increase in polar uncharged amino acids suggests that hydrogen bonds form between the peptides and the metal oxide surface. The peptides expressed on the hematite-binding phage also contained approximately twice the expected frequency of proline, serine, and threonine (Table 1).

Although serine and threonine are able to form hydrogen bonds, proline is known to be a highly disruptive residue that introduces bends into a polypeptide chain. This is due to the backbone-coupled pyrrolidine ring that restricts the flexibility of proline. For the random Ph.D.-12 library, proline has an expected frequency of 6%; however, we observed proline residues within our peptides at a frequency of 11% (Table 1). The fact that our observed proline frequency was one standard deviation higher than the expected frequency (Table 1), and the fact that proline was observed at a specific location within the hematite-binding peptide sequences (Figure 1), suggested that peptides having a Ser/Thr-Pro-Ser/Thr sequence take on a structural conformation that confers a higher affinity for the hematite surface.

To test this hypothesis, we carried out molecular dynamics simulations of the interaction between a hematite surface and the tripeptide sequence Ser-Pro-Ser. The peptide sequence Ser-Gly-Ser was used as a control. The achiral amino acid glycine (Gly) was chosen as the spacer amino acid in

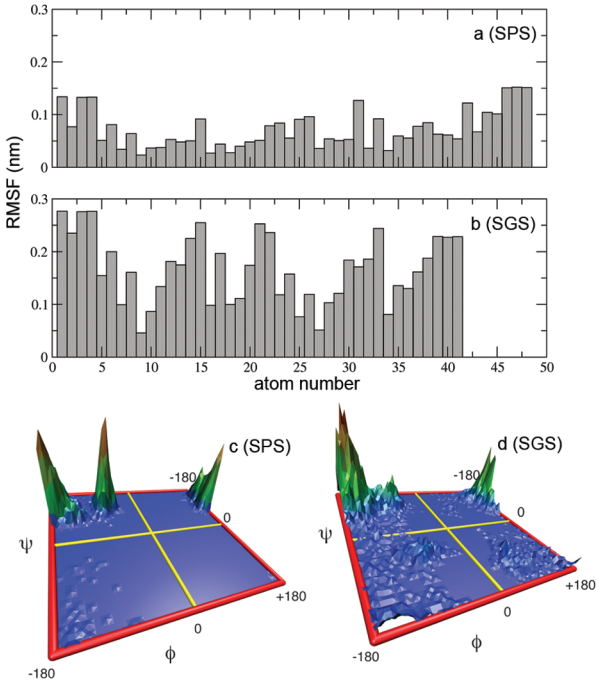

FIGURE 2. Root mean square fluctuations (RMSF) for the (a) SPS peptide and (b) SGS peptide atoms and corresponding Ramachandran distrbutions (c: SPS; d: SGS). Results are shown for the 2.5−5.0 ns interval.

our control tripeptide because it has a hydrogen atom as a side chain R group and is therefore exempt from many steric restrictions that the other 19 naturally occurring amino acids experience.

An all-atom root-mean-square fluctuation (RMSF) was used to assess the degree of order that proline, in comparison to glycine, imposed on the tripeptide sequence (Figure 2, panels a and b). The RMSF was used to quantitatively compare the structures of the two peptides (SPS vs SGS) bound to the hematite surface by measuring the deviation of the peptide's structure from its initial conformation. It is worth noting that the RMSF profiles are for the peptides adsorbed at the mineral surface, rather than peptides that are free in solution. As seen in Figure 2, the SPS peptide structure remains closer to its starting conformation when bound to hematite than does the SGS peptide. The RMSF plots show significantly lower peptide flexibility when proline is used as spacer ($RMSF_{SPS} = 0.072$ nm $\pm$ 0.036) versus glycine ($RMSF_{SGS} = 0.167$ nm $\pm$ 0.064). Also note that this lack of flexibility is propagated throughout the atoms of the entire SPS molecule rather than being restricted to only the atoms of proline (Figure 2a).

Ramachandran plots were constructed (Figure 2, panels c and d) to examine the possible conformations of SPS and SGS. These plots describe an amino acid's ability to rotate about the N−C_α and C_α−C bonds within the N−C_α−C peptide backbone. This rotation is restricted by steric interactions between main- and side-chain atoms of adjacent amino acid residues. The angle denoted ϕ (phi) describes the rotation about the N−C_α bond of an amino acid, whereas the ψ (psi) angle denotes rotation about the bond linking the C_α and the carbonyl carbon. Because rotation about the peptide bond is intrinsically limited by its double-bonded nature, the conformation freedom of an amino acid contained within a peptide can be describe by ϕ and ψ. Ramachandran plots are a way to visualize the possible ϕ and ψ backbone torsional angles for each residue in a peptide. Clockwise angles are positive and counterclockwise angles are negative, with each torsional angle ranging from −180° to +180°. A peptide having high conformational diversity can adopt ϕ and ψ values in all four quadrants of the Ramachandran plot, whereas a peptide having a limited number of possible combinations of ϕ and ψ will populate far less area of the Ramachandran plot.

The Ramachandran distributions for these simulations show that proline has a dramatic impact on the conformational diversity of the peptides when it is in contact with the mineral surface (Figure 2c). Unlike the Ramachandran distribution for the SGS peptide (Figure 2d), three clearly distinct peaks can be seen for SPS (Figure 2c). Two peaks correspond to proline, $\phi = -71.3° \pm 13.5$ and $\psi = 139.6° \pm 29.4$, and a third peak crosses the quadrant sign with ϕ and ψ values around +/−180°, corresponding to the serine residues. The kink introduced by proline's ϕ torsional angle results in an arched tripeptide structure with extended serine residues at its ends ($\phi = \psi = +/-180°$ would produce a perfectly extended SPS conformation). These results suggest that proline restricts the peptide conformational sampling when in contact with the mineral surface, resulting in a favorable hematite-binding motif. By locking the two serine amino acids in place, it appears that the peptide is able to template the hydroxylated hematite surface in a manner that promotes hydrogen bonding between the hydroxyl groups of both serine amino acids and hydroxyl groups on the mineral surface.

This notion is supported by the fact that SPS was bound to the mineral surface during the entire simulation (Figure 3, panels a and b; also see the Supporting Information), unlike SGS, which began to release from hematite after approximately 2.5 ns (Figure 3c−e; also see the Supporting Information). You can clearly see in Figure 3a that the minimum distance between atoms in SPS is relatively constant throughout the entire 5 ns simulation, although it should be pointed out that proline in SPS does exhibit some variability in its distances between atoms at approximately 2.5 ns, but these variations return to stable values at approximately 3.0 ns and remain relatively constant for the rest of the simulation. By comparison, the minimum distance between atoms in SGS is fairly constant up until approximately 2.5 ns, when Ser II and Gly exhibit large fluctuations in their minimum distance values (Figure 3c). Note that in Figure 3, a snapshot is shown for the SGS−hematite simulation at 2.0 ns (Figure 3d); however, no snapshot is shown for the SPS−hematite simulation at 2 ns. This is because, unlike the simulation for SGS−hematite, both serine residues of SPS remain bound to the mineral surface via hydrogen bonds during the entire simulation; therefore, the snapshot for SPS−hematite at 2 ns is identical to that obtained for SPS−hematite at 5 ns (Figure 3b).

Given the observed configuration of SPS at the hematite surface, we can speculate that other residues having restricted access to the configurational space such as (i) β-branched valine, isoleucine, and threonine and (ii) residues containing large side chains, such as leucine and tryptophan, may also serve as suitable hydroxide-spacer residues (e.g., SIS, STS) that confer similar metal-oxide binding properties. In fact, our phage peptides 2, 4, 6, 12, and 15 (Figure 1) have their C-terminal hydroxyl amino acids separated by leucine, isoleucine, tryptophan, valine, and leucine, respectively. Figure 1 also shows that 90% of the hematite-binding phage contained a universally conserved bulky-hydrophobic residue (see # symbol, Figure 1), which separated adjacent hydroxyl amino acids.

As suggested in the introduction, the general premise of this research was to investigate whether or not phage display technology could be used on a much shorter time scale to mimic the natural selection that occurs in nature. Therefore, we compared the amino-acid motif shown in Figure 1 to published sequences of microbial proteins that are known to interact with metal oxides, specifically OmcA and MtrC

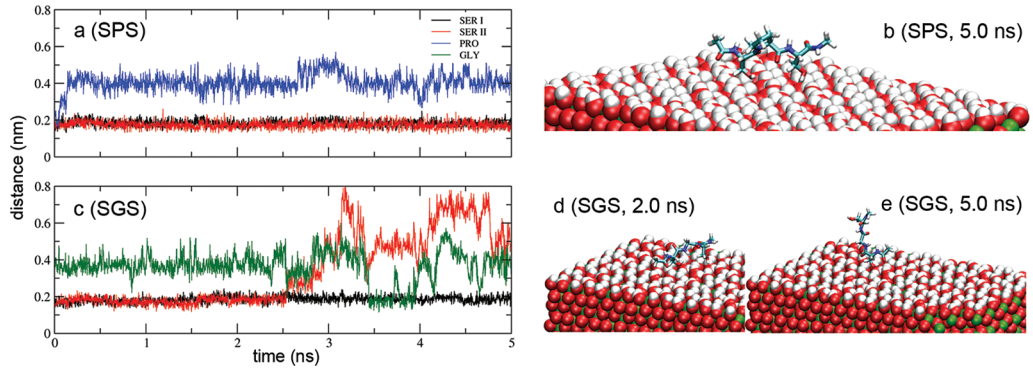

FIGURE 3. Peptide−hematite surface adhesion as a function of time. Minimum distance between any atom of (a) SPS and (c) SGS peptides and the mineral surface (results displayed for each residue). Snapshot of (b) the SPS-hematite simulation at 5 ns, and snapshots of the SGS-hematite simulation at (d) 2 ns and (e) 5 ns. The hematite slab is represented in the CPK model and the peptides as stick models. Atoms in molecular representations (b, d, and e) are colored as followed: iron, green; oxygen, red; hydrogen, white; carbon, cyan; nitrogen, blue.

from the metal-reducing bacterium *S. oneidensis* MR-1. We also employed the ScanProsite tool (http://ca.xpasy.org) to scan our metal-oxide binding motif against the UniProtKB/Swiss-Prot databases.

S. oneidensis MR-1 outer membrane cytochromes OmcA and MtrC (also known as OmcB) have been shown to bind to the metal-oxide hematite (*6, 7, 32*). Furthermore, these cytochromes are believed to catalyze the terminal reduction of iron oxides by transferring electrons directly from the bacterial cell to the mineral surface during anaerobic respiration (*1, 6, 7, 11, 32, 33*). Upon close inspection of the primary sequences of both OmcA and MtrC, it is interesting to note that although neither cytochrome contains the 5-amino acid motif Ser/Thr-hydrophobic/aromatic-Ser/Thr-Pro-Ser/Thr, each of the proteins does have the 3-amino acid motif, Ser/Thr-Pro-Ser/Thr (i.e., the tripeptide that we used in our molecular dynamics simulations), which is observed once in each cytochrome. For both OmcA and MtrC, Ser/Thr-Pro-Ser/Thr is found at the protein's C-terminus and is adjacent to the terminal heme X binding domain (i.e., CXXCH). The C-terminal sequence for OmcA is **CATCHTPS** QLMEAHGN$_{735}$ and for MtrC is **CFYCHTPT**VADHTKVKM$_{671}$.

The proximity of the Ser/Thr-Pro-Ser/Thr and heme-binding domain is noteworthy given a recent publication by Kerisit et al. (*33*), who conducted molecular dynamic simulations of hematite and the small tetraheme cytochrome from *S. oneidensis*. The small tetraheme cytochrome was selected by Kerisit et al. (*33*) as a model for OmcA or MtrC because of the lack of structural information for the larger decaheme cytochromes (i.e., OmcA and MtrC). In 89% of their simulations, a terminal heme (i.e., heme I or IV) was found to bind to the hematite surface, and in 75% of their simulations, where at least one heme was in contact with the hematite surface, they found that the heme's propionate groups were responsible for forming a strong hydrogen bond with the mineral surface (*33*). The similarities between our study and that of Kerisit et al. (*33*) suggest that Ser/Thr-Pro-Ser/Thr within MtrC and OmcA may help orientate the cytochrome molecules such that the terminal heme (i.e., heme X) is in direct contact with the hematite surface, which would in turn facilitate the terminal electron transfer between the cytochromes and mineral.

A further search using a computer database (UniProtKB/Swiss-Prot) revealed that our hematite-binding motif was also contained within the primary sequence of silaffins, which are a group of metal-oxide binding proteins/peptides. This was a rather curious discovery, as silaffins do not necessarily interact with iron oxides like hematite. Rather, silaffins are found in the cell walls of unicellular eukaryotic algae, commonly referred to as diatoms (*12, 13, 34*), and are biosilica-associated proteins/peptides that are rich in serine, threonine, proline, and hydroxyproline (*12−15, 34−40*). These proteins have been shown to induce rapid silica (SiO_2) deposition in vitro and to control the nanostructure of the forming silica (*12−15*). It has been hypothesized that silaffins regulate silica formation in diatoms and act as templates that mediate biosilica nanopatterning (*14, 15*).

It is a bit surprising that both minerals would share similar peptide-binding motifs because the point of zero charge for silica and hematite are very different (silica ~2 and hematite 7−9). However, both minerals display a hydroxyl-rich surface capable of multiple hydrogen bond interactions. As shown by our molecular simulations, this is the driving force between SPS adhesion to hematite. Furthermore, the importance of hydrogen bonding was also demonstrated by the phage binding experiments in which we showed that a hydroxyl-rich peptide, LSTVQTISPSNH (phage No. 19), could readily bind to hematite, whereas a hydroxyl-less peptide, GHANHQAWNNLA, could not bind to the surface of hematite. It is beyond the scope of this paper to conduct binding experiments and molecular dynamic simulations with silica or quartz minerals. Nonetheless, it is certainly interesting that our hematite-binding phage display a motif that is similar to peptides that interact with silica.

Two silaffins in particular, Sil1 and Sil2 from *Thalassiosira pseudonana* (*12, 13*), contain the amino acid consensus sequence, Ser/Thr-hydrophobic/aromatic-Ser/Thr-Pro-Ser/Thr, which is identical to the C-terminus of our conserved hematite-binding motif (Table 2). Even more interesting, this 5-amino-acid consensus sequence is repeated multiple times in the primary sequences of these proteins (Table 2). In Sil1, this motif is repeated eight times, and in Sil2, Ser/Thr-hydrophobic/aromatic-Ser/Thr-Pro-Ser/Thr is repeated nine times (Table 2). This leads us to hypothesize that these conserved motif repeats constitute a natural silica-binding domain, which through the evolution of these microorganisms, has developed within the primary sequences of Sil1 and Sil2 to function in silica biomineralization. Others have also proposed that these consensus sequence repeats function as a peptide template for mediating biosilica nanopatterning (*12, 13*).

Furthermore, for Sil1, the sequence Ser/Thr-Pro-Ser/Thr is observed 24 times, and Ser/Thr-hydrophobic/aromatic-Ser/Thr is observed 17 times. In Sil2, Ser/Thr-Pro-Ser/Thr is observed 19 times and Ser/Thr-hydrophobic/aromatic-Ser/Thr is observed 15 times. These observations support our previous argument that residues with limited access to the configurational space, when placed between hydroxyl residues, lock the peptide into an extended-like configuration, which allows the peptide to more efficiently bind to and

TABLE 2. Comparison of the C-terminal Conserved Hematite Binding Motif of Our Phage Peptides to the Metal-Oxide Binding Proteins Sil1 and Sil2 from *Thalassiosira pseudonana*

C-terminal hematite binding motif	S/T	#[a]	S/T	P	S/T
Sil1	T_{187}	A	S	P	T_{191}
Sil1	T_{263}	L	S	P	S_{267}
Sil1	S_{301}	A	S	P	T_{305}
Sil1	T_{325}	L	S	P	T_{329}
Sil1	T_{333}	L	S	P	T_{337}
Sil1	S_{341}	L	S	P	T_{345}
Sil1	T_{349}	W	S	P	T_{353}
Sil1	T_{407}	I	S	P	T_{411}
Sil2	T_{187}	A	S	P	T_{191}
Sil2	T_{247}	F	T	P	T_{251}
Sil2	T_{262}	L	S	P	S_{266}
Sil2	S_{300}	A	S	P	T_{304}
Sil2	T_{320}	L	S	P	T_{324}
Sil2	S_{328}	L	S	P	T_{332}
Sil2	T_{332}	L	S	P	T_{336}
Sil2	T_{336}	W	S	P	T_{340}
Sil2	T_{394}	I	S	P	T_{398}

[a] Nonpolar hydrophobic, including aromatic, amino acids.

template the metal oxide surface. As mentioned above, in addition to proline, hydroxyproline is also abundant in the cell-wall proteins/peptides of diatoms (*34*−*40*). The reduced flexibility conferred by the imidazole ring in hydroxyproline has been shown to afford hydroxyproline the same conformational restrictions as proline (*35, 37, 39, 40*). Therefore, we speculate that hydroxyproline plays a similar role to proline in these proteins/peptides.

A number of previous studies, including those referenced above, have shown that microorganisms evolved the ability to synthesize a diverse assortment of macromolecules (e.g., proteins) with a high affinity for specific inorganic mineral phases (*12, 13, 32, 33, 41*−*44*). Here we attempted to mimic this type of evolutionary selection by using phage-display technology to select from billions of different sequences those peptides that bind to a specific oxide mineral (i.e., Fe_2O_3). We identified an amino-acid motif that appears to provide specificity toward the mineral. Molecular dynamics simulations of the peptide-mineral interactions show that the peptide specificity is conferred in part by sequences of proline or β-branched residues placed between adjacent hydroxyl residues. This structural sequence restricts the peptide flexibility, thereby inducing a structural metal-oxide binding motif. Searching the literature for known or putative metal-oxide binding proteins revealed that our metal-oxide binding motif is present in at least four metal-oxide-binding proteins. These include OmcA and MtrC, which have been shown to bind to Fe_2O_3 (*6, 7, 32*) and Sil1 and Sil2, which have been shown to bind to SiO_2 (*12*−*15*). These results suggest that all or part of amino-acid motif discovered here may constitute a natural metal-oxide binding archetype. Such an archetype could be exploited in the design of enzyme-based biofuel cells and approaches to synthesize tailored metal-oxide nanostructures.

Acknowledgments

We acknowledge the support of the U.S. Department of Energy (DOE) OBES Geosciences Research Program and the DOE Office of Advanced Scientific Computing Research. Gratitude is also expressed to the W. R. Wiley Environmental Molecular Sciences Laboratory (EMSL) through the Computational Grand Challenge Application GC20892. S. K. L acknowledges NSF grant EAR-0525297. M. F. H. acknowledges DOE grant DE-FG02-06ER15786 and NSF IGERT grant DGE-0504196. R. D. L. thanks S. Kerisit for providing the atomic coordinates of the hematite surface. Part of this research was conducted at EMSL, a national scientific user facility sponsored by the DOE OBER program located at Pacific Northwest National Laboratory (PNNL). PNNL is operated for the DOE by Battelle Memorial Institute under Contract DE-AC05-76RLO1830. We also thank three anonymous reviewers for their insightful comments.

Supporting Information Available

Supporting Information is offered for this research. This information is available free of charge via the Internet at http://pubs.acs.org.

Literature Cited

(1) Nealson, K. H.; Saffarini, D. Iron and manganese in anaerobic respiration: Environmental significance, physiology, and regulation. *Annu. Rev. Microbiol.* **1994**, *48*, 311–343.
(2) Vargas, M.; Kashefi, K.; Blunt-Harris, E. L.; Lovley, D. R. Microbiological evidence for Fe(III) reduction on early Earth. *Nature* **1998**, *395*, 65–67.
(3) Bond, D. R.; Lovley, D. R. Electricity production by *Geobacter sulfurreducens* attached to electrodes. *Appl. Environ. Microbiol.* **2003**, *69*, 1548–1555.
(4) Rabaey, K.; Boon, N.; Siciliano, S. D.; Verhaege, M.; Verstraete, W. Biofuel cells select for microbial consortia that self-mediate electron transfer. *Appl. Environ. Microbiol.* **2004**, *70*, 5373–5382.
(5) Kim, J. R.; Min, B.; Logan, B. E. Evaluation of procedures to acclimate a microbial fuel cell for electricity production. *Appl. Microbiol. Biotechnol.* **2005**, *68*, 23–30.
(6) Xiong, Y.; Shi, L.; Chen, B.; Mayer, M. U.; Lower, B. H.; Londer, Y.; Bose, S., Jr.; Fredrickson, J. K. High-affinity binding and direct electron transfer to solid metals by the *Shewanella oneidensis* MR-1 outer membrane c-type cytochrome OmcA. *J. Am. Chem. Soc.* **2006**, *128*, 13978–13979.
(7) Eggleston, C. M.; J, V.; Shi, L.; Lower, B. H.; Droubay, T. C.; Colberg, P. J. S. Binding and direct electrochemistry of OmcA, an outer-membrane cytochrome from an iron reducing bacterium, with oxide electrodes: A candidate biofuel cell system. *Inorg. Chim. Acta* **2008**, *361*, 769–777.
(8) Kim, J.; Jia, H.; Wang, P. Challenges in biocatalysis for enzyme-based biofuel cells. *Biotechnol. Adv.* **2006**, *24*, 296–308.
(9) Davis, F.; Higson, S. P. Biofuel cells—Recent advances and applications. *Biosens. Bioelectron.* **2007**, *22*, 1224–1235.
(10) Smith, G. P.; Petrenko, V. A. Phage display. *Chem. Rev.* **1997**, *97*, 391–410.
(11) Myers, C. R.; Myers, J. M. The outer membrane cytochromes of *Shewanella oneidensis* MR-1 are lipoproteins. *Lett. Appl. Microbiol.* **2004**, *39*, 466–470.
(12) Poulsen, N.; Kroger, N. Silica morphogenesis by alternative processing of silaffins in the diatom *Thalassiosira pseudonana*. *J. Biol. Chem.* **2004**, *279*, 42993–42999.
(13) Poulsen, N.; Sumper, M.; Kroger, N. Biosilica formation in diatoms: characterization of native silaffin-2 and its role in silica morphogenesis. *Proc. Natl. Acad. Sci.* **2003**, *100*, 12075–12080.
(14) Kroger, N.; Lorenz, S.; Brunner, E.; Sumper, M. Self-assembly of highly phosphorylated silaffins and their function in biosilica morphogenesis. *Science* **2002**, *298*, 584–586.
(15) Sumper, M.; Kroger, N. Silica formation in diatoms: the function of long-chain polyamines and silaffins. *J. Mater. Chem.* **2004**, *14*, 2059–2065.
(16) Stipp, S. L., Jr. Structure and bonding environments at the calcite surface as observed with X-ray photoelectron-spectroscopy (XPS) and low-energy electron-diffraction (LEED). *Geochim. Cosmochim. Acta* **1991**, *55*, 1723–1736.
(17) Parmley, S. F.; Smith, G. P. Antibody-selectable filamentous fd phage vectors: Affinity purification of target genes. *Gene* **1988**, *73*, 305–318.
(18) Cornell, W. D.; Cieplak, P.; Bayly, C. I.; Gould, I. R.; Merz, K. M.; M, F. D.; Spellmeyer, D. C.; Fox, T.; Caldwell, J. W.; Kollman, P. A. A 2nd generation force-field for the simulation of proteins, nucleic-acids, and organic-molecules. *J. Am. Chem. Soc.* **1995**, *117*, 5179–5197.
(19) Straatsmaz T. P. *NWChem-4.7*, 5.0 ed., Laboratory, P. N. N., Ed.: Richland, Washington, 2003.
(20) Lins, R. D.; Hunenberger, P. H. A new GROMOS force field for hexopyranose-based carbohydrates. *J. Comput. Chem.* **2005**, *26*, 1400–1412.

(21) Kerisit, S.; Rosso, K. M. Computer simulation of electron transfer at hematite surfaces. *Geochim. Cosmochim. Acta* **2006**, *70*, 1888–1903.

(22) Trainor, T. P.; Chaka, A. M.; Eng, P. J.; Newville, M.; Waychunas, G. A.; Catalano, J. G., Jr. Structure and reactivity of the hydrated hematite (0001) surface. *Surf. Sci.* **2004**, *573*, 204–224.

(23) Eggleston, C. M.; Stack, A. G.; Rosso, K. M.; Higgins, S. R.; Bice, A. M.; Boese, S. W.; Pribyl, R. D.; Nichols, J. J. The structure of hematite (α-Fe_2O_3) (001) surfaces in aqueous media: Scanning tunneling microscopy and resonant tunneling calculations of coexisting O and Fe terminations. *Geochim. Cosmochim. Acta* **2003**, *67*, 985–1000.

(24) Parker, S. C.; de Leeuw, N. H.; Redfern, S. E. Atomistic simulation of oxide surfaces and their reactivity with water. *Faraday Discuss.* **1999**, *114*, 381–393.

(25) Spagnoli, D.; Cooke, D. J.; Kerisit, S.; Parker, S. C. Molecular dynamics simulations of the interaction between the surfaces of polar solids and aqueous solutions. *J. Mater. Chem.* **2006**, *16*, 1997–2006.

(26) Liu, P.; Kendelewicz, T., Jr.; Nelson, E. J.; Chambers, S. A. Reaction of water vapor with α-Al_2O_3(0001) and α-Fe_2O_3(0001) surfaces: Synchrotron X-ray photoemission studies and thermodynamic calculations. *Surf. Sci.* **1998**, *417*, 53–65.

(27) Berendsen, H. J. C.; Postma, J. P. M.; Vangunsteren, W. F.; Dinola, A.; Haak, J. R. Molecular-dynamics with coupling to an external bath. *J. Chem. Phys.* **1984**, *81*, 3684–3690.

(28) Essmann, U.; Perera, L.; Berkowitz, M. L.; Darden, T.; Lee, H.; Pedersen, L. G. A smooth particle mesh Ewald method. *J. Chem. Phys.* **1995**, *103*, 8577–8593.

(29) Ryckaert, J. P.; Ciccotti, G.; Berendsen, H. J. C. Numerical-integration of cartesian equations of motion of a system with constraints-molecular dynamics of N-alkanes. *J. Comput. Phys.* **1977**, *23*, 327–341.

(30) Hockney, R. W. The potential calculation and some applications. *Meth. Comput. Phys.* **1970**, *9*, 135–211.

(31) Livingstone, C. D.; Barton, G. J. Protein sequence alignments: a strategy for the hierarchical analysis of residue conservation. *Comput. Appl. Biosci.* **1993**, *9*, 745–756.

(32) Lower, B. H.; Shi, L.; Yongsunthon, R.; Droubay, T. C.; McCready, D. E.; Lower, S. K. Specific bonds between an iron oxide surface and outer membrane cytochromes MtrC and OmcA from *Shewanella oneidensis* MR-1. *J. Bacteriol.* **2007**, *189*, 4944–4952.

(33) Kerisit, S.; Rosso, K. M.; Dupuis, M.; Valiev, M. Molecular computational investigation of electron-transfer kinetics across cytochrome-iron oxide interfaces. *J. Phys. Chem. C* **2007**, *111*, 11363–11375.

(34) Kroger, N.; Bergsdorf, C.; Sumper, M. Frustulins: Domain conservation in a protein family associated with diatom cell walls. *Eur. J. Biochem.* **1996**, *239*, 259–264.

(35) Cartier, L.; Lotz, B. Frustrated crystal structure of poly(L-hydroxyproline). *Macromolecules* **1998**, *31*, 3049–3054.

(36) Kroger, N.; Bergsdorf, C.; Sumper, M. A new calcium-binding glycoprotein family constitutes a major diatom cell-wall component. *EMBO J.* **1994**, *13*, 4676–4683.

(37) Nakajima, T.; Volcani, B. E. 3,4-dihydroxyproline — A new amino acid in diatom cell walls. *Science* **1969**, *164*, 1400–1401.

(38) Hecky, R. E.; Mopper, K.; Kilham, P.; Degens, E. T. Amino-acid and sugar composition of diatom cell-walls. *Mar. Biol.* **1973**, *19*, 323–331.

(39) Karle, I. L. Structure of a new natural amino acid, 2,3-cis-3,4-trans-3,4-dihydroxy-L-proline. *Acta. Crystall. B-Stru.* **1970**, *B26*, 765–770.

(40) Sasisekharan, V. Structure of poly-L-hydroxyproline-A. *Acta Crystallogr.* **1959**, *12*, 903–909.

(41) Arakaki, A.; Webb, J.; Matsunaga, T. A novel protein tightly bound to bacterial magnetic particles in *Magnetospirillum magneticum* strain AMB-1. *J. Biol. Chem.* **2003**, *278*, 8745–8750.

(42) Lower, S. K.; Hochella, M. F., Jr.; Beveridge, T. J. Bacterial recognition of mineral surfaces: Nanoscale interactions between *Shewanella* and alpha-FeOOH. *Science* **2001**, *292*, 1360–1363.

(43) Lower, B. H.; Hochella, M. F., Jr.; Lower, S. K. Putative mineral-specific proteins synthesized by a metal reducing bacterium. *Am. J. Sci.* **2005**, *305*, 687–710.

(44) Schultze-Lam, S.; Harauz, G.; Beveridge, T. J. Participation of a cyanobacterial S layer in fine-grain mineral formation. *J. Bacteriol.* **1992**, *174*, 7971–7981.

ES702688C